PROCEEDINGS, Thirty-Eighth Workshop on Geothermal Reservoir Engineering
Stanford University, Stanford, California, February 11-13, 2013
SGP-TR-198

PHENOMENOLOGICAL STUDY OF TEMPERATURE GRADIENT ANOMALIES IN THE BUNTSANDSTEIN FORMATION, ABOVE THE SOULTZ GEOTHERMAL RESERVOIR, USING TOUGH2 SIMULATIONS

Deborah Siffert[1], Sébastien Haffen[2], Michel H. Garcia[1], Yves Géraud[2]

[1]KIDOVA
155 avenue Roger Salengro
92340 Chaville, France
E-mail: deborah.siffert@kidova.com, michel.garcia@kidova.com

[2] ENSG – Université de Lorraine
Rue du Doyen Marcel Roubault
54500 Vandœuvre-les-Nancy, France
E-mail: shaffen@unistra.fr, yves.geraud@univ-lorraine.fr

ABSTRACT

The geothermal reservoir at Soultz-sous-Forêts occurs in a granite horst bounded by subvertical normal faults. Exploration and production results tend to show that the Buntsandstein formation, made of inter-bedded sandstones and argillite in the Rhine Graben, above the granitic basement, may also have geothermal potential. Indeed, temperature gradient anomalies observed in the Buntsandstein indicate that the Buntsandstein could be exploited to produce heat or even electricity.

Anomalies of temperature gradient observed in wells could be explained by fluid flow patterns related to the faults. In order to validate this hypothesis, a phenomenological study was carried out using TOUGH2 to simulate fluid flow and heat transfer for various boundary conditions. The results of this study demonstrate that the anomalies could only be explained by lateral flows connecting two faults through three litho-stratigraphic levels identified as possible fluid circulation zones from petrophysical analyses. The differential of hydraulic potential gradient, from one fault to the other, required to allow geothermal fluids to flow inside the rock formation, can be explained by a structural dip of about 3°, consistent with observations at Soultz-sous-Forêts.

INTRODUCTION

The geothermal power plant of Soultz-sous-Forêts is located in the east of France, at the western part of the Rhine Graben. It produces electricity from the heat present in a 5,000 m deep fractured granite reservoir (Genter et al., 2000). Based on exploration results of the region, several geothermal projects have been started to exploit the Rhine Graben reservoir. Most of them target the sandstones or the interface between sandstones and granite (Rittershoffen in France, Landau in Germany). Studies were carried out to evaluate the geothermal potential of the Buntsandstein formation, located above the granite basement, between 1,000 and 1,400 m depth at Soultz-sous-Forêts (Dezayes et al., 2007). Provided this formation is a good enough aquifer and is sufficiently connected to the granite reservoir, it could directly be exploited to produce geothermal energy at significantly lower drilling costs. In order to confirm this assumption, a temperature log, covering both the granites and the overlying Triassic sediments, was analyzed as well as the temperature gradient derived from it. This analysis shows that the temperature gradient is lower than initially expected, from the upper part of the granite reservoir through the overlying Buntsandstein formation, thus leading to high temperatures in this formation. Based on these results and others obtained from Soultz geothermal operations, additional studies were initiated to target the Buntsandstein formation to produce heat or electricity.

Previous works showed that the thermal anomaly in the Rhine graben can be related to vertical circulation of thermal water along faults (Bächler, 2003; Kohl, 2000). In order to characterize the fluid flow pattern and the heat diffusion and convection processes in sandstones, petrophysical properties were measured on cores from borehole EPS1 (Soultz-sous-Forêts, France). The results of the comparison between theoretical and measured temperature gradient logs suggest that fluid flows exist and are localized in the fault zones and also in several matrix layers (Haffen, 2012; Haffen et al., 2013).

This paper presents the two-part work that was carried out to first identify the permeable layers where fluids are likely to flow in the Buntsandstein formation, then to demonstrate numerically that only inter-fault flows through these layers could explain the temperature gradient anomalies. The permeable layers were identified by comparing the theoretical thermal gradient with the measured one, on the one hand, and by comparing the petrophysical properties and the fracture densities inside and outside the discrepancy zones, on the other hand. Based on these observations, a simplified 2D vertical conceptual model was defined that integrates the different horizontal lithostratigraphic layers, associated with petrophysical properties measured on cores, and is bounded laterally with two vertical faults. Several flow and heat transport simulations were carried out using TOUGH2 (Pruess, 1999), based on different flow and (prescribed) temperature boundary conditions. This phenomenological study was conducted to better understand the hydrogeological system of Rhine graben.

SURFACE AND WELL LOG DATA

Geological and Petrophysical Settings

The sandstone formation of Buntsandstein is a widespread formation in Europe, but has a particular structure in the Rhine graben. The Upper Rhine Graben system, oriented NNE-SSW (Figure 1a and 1b), has been structured during two main periods of extension of the Late Eocene and Oligocene and shearing since Miocene.

The different formations are crossed by several sets of major (extended) faults (Genter *et al.* 2000). Two main fault sets could be observed in the Upper Rhine Graben: variscan and alpine sets. These structures divide the various formations into 100 to 1,000 m wide blocks. The Buntsandstein sandstone is one of these compartimentalized formations, below the Muschelkalk and above the granite basement.

In order to study flow and heat transfer processes in the Buntsandstein, various petrophysical parameters were measured on cores from the various rock types present in the reservoir. Measured porosity, permeability and acoustic velocity data were used to characterize the structures and textures of sandstones that control fluid flows. Thermal conductivities were also measured for each layer, as required to compute or simulate heat transfers. The measurements were performed by Haffen (2012), Sizun (1995) and Vernoux (1995), on several outcrop rock samples and on cores from EPS-1 (Figure 1c), which is the only borehole cored from 930 m in the Muschelkalk, to 2,220 m in the granite (see also associated paper of Haffen *et al.*, 2013b, in this volume).

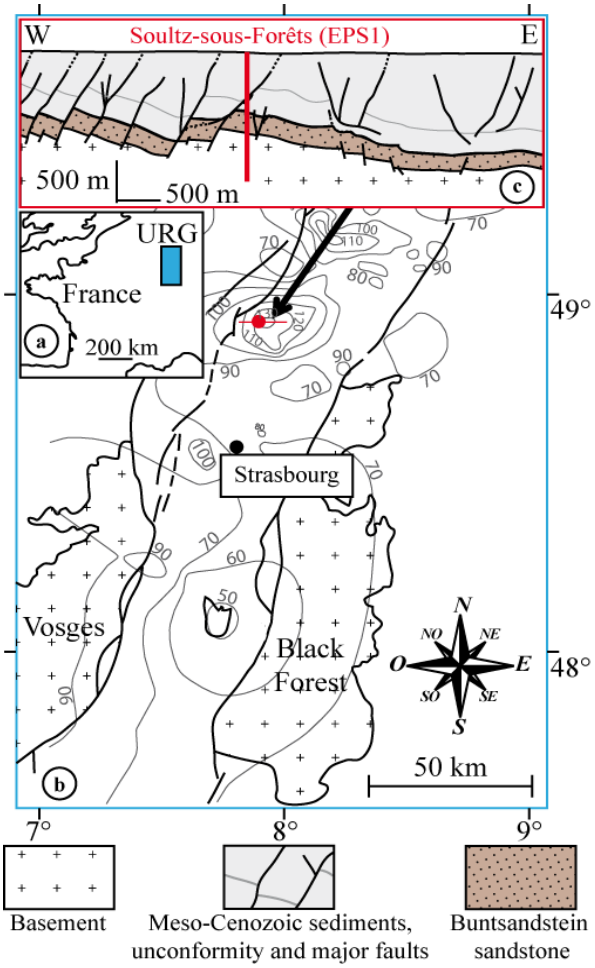

Figure 1: (a) Location of the Upper Rhine Graben (URG) in Western Europe. (b) URG map [modified from Schumacher (2002)]; the red dot and line located at Soultz-sous-Forêts denote the locations of borehole EPS1 and the geological cross-section. The grey lines indicate the temperature at 1,500 m depth based on data from GGA Hannover (Genter et al., 2004; Pribnow and Schellschmidt, 2000). (c) Soultz-sous-Forêts geological cross-section [redrawn after Place et al. (2010)] showing the approximate path of borehole EPS1.

Thermal Investigations

The geothermal gradient measured at Soultz-sous-Forêts is 105°C/km in the Upper Triassic levels and progressively decreases through the Buntsandstein and the upper granitic basement (Figure 2). The geothermal gradient increases again, starting at 3,000 m depth. This could be explained by both the contrast of thermal conductivities, between the sedimentary cover and the granite, and the presence of natural conductive heat transfer levels at the top of the granite (Le Carlier et al., 1994).

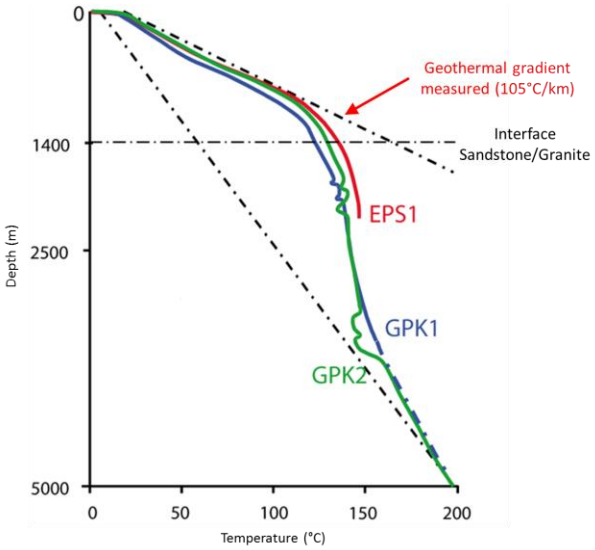

Figure 2: Thermal gradients measured at Soultz-sous-Forêts, according to Pribnow et al. (1999).

As a first evaluation of the fluid flow pattern within the sandstone formation, analytical (theoretical) and measured geothermal gradient logs were compared. The analytical one was calculated using the thermal conductivity data, the Fourier law, and relevant temperature boundary conditions at the top and bottom of the formation. The measured one was derived from the temperature log measured along borehole EPS1. If the heat fluxes are only due to diffusion processes, calculated and observed temperature gradient logs are expected to be similar. If convection processes are also involved, resulting from fluid flows through the fault system connecting the granite basement to the overlying Buntsandstein formation, discrepancies should be observed between the two logs.

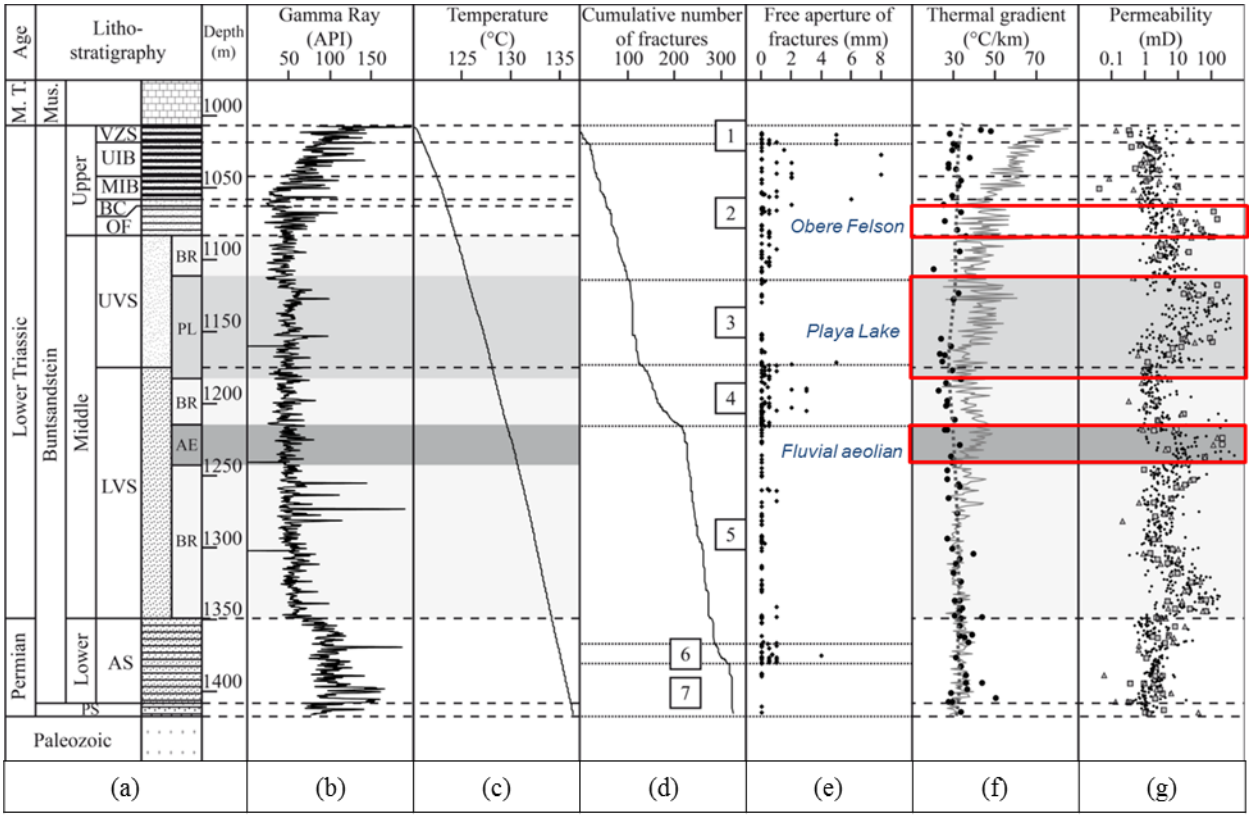

Figure 3: Qualitative analysis of the petrophysical data to estimate the flow pattern in the sandstone reservoir (modified from Haffen, 2012). (a) Stratigraphic column of borehole EPS1 (Sizun, 1995)(MT: Middle Triassic, Mus.: Muschelkalk, VZS: Voltzia Sandstones, UIB: Upper Intermediate Buntsandstein, MIB:Median Intermediate Buntsandstein, BC: Bitche Conglomerate, OF: Obere Felson, UVS: Upper Vosgian Sandstones, LVS: Lower Vosgian Sandstones, AS: Annweiller Sandstones, PS: Permian Sandstones), (b) Gamma-ray log. (c) Temperature log, (d) Cumulative number of fractures, (e) Free aperture of fractures, (f) Geothermal gradients (black points = theoritical gradient, grey curve = measured gradient), (g) Permeability measured parallel and perpendicular to stratification.

As shown in Figure 3 the measured geothermal gradient is higher than the theoretical one in two zones: 1) in and near layers of higher permeabilities (Obere Felson, Playa-Lake and Fluvio-Aeolian marginal erg facies), 2) in layers containing open fractures (Upper Buntsandstein). From these observations, it was inferred that a fluid flow network, somehow involving the sub-vertical faults and the permeable sedimentary layers, should be present (see associated paper of Haffen et al., 2013b, for further details). The aim of the phenomenological study was to determine which flow conditions, applying to the crossing faults, could explain the observed geothermal gradient departures. This is the purpose of the next section.

CONCEPTUAL AND NUMERICAL MODELS

Conceptual Model at the Fault Block Scale

The Buntsandstein formation is interpreted as being comprised of fault blocks. The data acquired in borehole EPS1 (Sizun, 1995) and from outcrops of the Rhine Graben were the basis for defining a representative fault block-scale conceptual model associated with petrophysical properties. This conceptual model consists of a 3D block bounded by two Variscan faults oriented N060° and two Rhenish faults oriented N020° (see associated paper of Haffen et al., 2013b for details). The thickness of faults and especially the extent of the damaged zone are variable, from 0.1 to 10 m (Caine et al., 1996). The study of various Rhine Graben outcrops shows that the Rhenish faults are surrounded by partially filled non-conductive fractures.

A simplified 2D form of this conceptual model was derived to conduct the phenomenological study using TOUGH2 flow and heat transport simulations for different boundary condition hypotheses. The objective being to identify flow paths through faults and permeable layers that can explain the temperature gradient anomalies, vertical faults and homogeneous horizontal layers were assumed (Figure 4). The model covers the Buntsandstein reservoir, from the Muschelkalk horizon at 980 m depth, and extends down to 14 m below the top of the granite reservoir at 1,416 m depth. The layers correspond to the main lithostratigraphic units identified in borehole EPS-1. The natural fracture network is ignored. The model is bounded on the left and the right by two vertical conductive faults 1,000 m apart. The fault thickness is assumed to be 1 m, according to Haffen (2012), who measured fault thicknesses ranging from 0.65 to 5 m, and the permeability is 0.01 mD, according to Place et al. (2010). The model is 1,000 m wide, 10 m thick and 450 m high. The corresponding TOUGH2 simulation grid is regular with 100 × 1 × 90 cells (Figure 4).

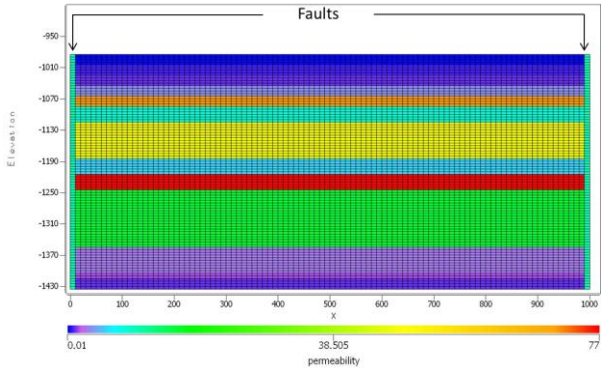

Figure 4: 2D numerical reservoir model (100×1×90 cells): layers and permeability (in mD).

Presentation of TOUGH2 Simulation Scenarios

Different boundary condition scenarios were studied to identify the ones that are likely to explain the temperature gradient anomalies observed in EPS1. The thermal boundary conditions are the same for all scenarios. They are simply defined as prescribed temperatures at the top and the bottom, according to those measured in EPS1, and no heat flux laterally. The flow boundary conditions are scenario-dependent with prescribed pressures applying to the top and bottom of each fault. Elsewhere, no flow is assumed for all scenarios.

Depending on the prescribed pressures applied to the faults, flows can be generated, or not, vertically, through the faults, and horizontally, through the permeable sedimentary layers. By so proceeding, three types of scenarios were considered.

Scenario 1: Hydrostatic conditions preventing fluids from flowing vertically from the granite reservoir through the faults.

This scenario corresponds to purely diffusive heat transfer and is equivalent to the analytical gradient calculated with the Fourier law and measured thermal conductivities.

Scenario 2: Same hydraulic potentials applied to the two faults, allowing vertical flows in the faults, but preventing fluids from flowing horizontally through the permeable sedimentary layers.

This scenario corresponds to two conductive but non-connected faults, convective heat transport only taking place within the faults.

Scenario 3: Different hydraulic potentials applied to the two faults, allowing both vertical flows in the faults and horizontal flows in the permeable sedimentary layers.

This scenario corresponds to two conductive faults that are connected through the permeable sedimentary layers, convective heat transport taking place within both the faults and the permeable layers.

Table 1 summarizes the prescribed pressure and temperature boundary conditions applied to each scenario.

Table 1: Pressure and temperature boundary conditions applied to the top and the bottom of the model for each scenario.

Scenario		*P (bar) left-hand fault*	*P (bar) right-hand fault*	*T (°C)*
1	Top BC	96		117
	Bottom BC	136		137
2	Top BC	96		117
	Bottom BC	140=136+4		137
3	Top BC	96	101=96+5	117
	Bottom BC	140=136+4	145=136+9	137

SIMULATION RESULTS

Comparison between Measured and Simulated Temperature Logs

The simulation of scenario 1 (purely diffusive heat transfer in hydrostatic conditions) is expected to show vertical temperature gradient logs similar to the analytical gradient calculated using the Fourier law. This is true far enough from the faults, the distribution of thermal conductivities being different inside and outside the faults in the numerical model. Figure 5 shows the two analytical and numerical (simulated) temperature gradient logs. The analytical gradient looks more erratic, with short scale variability, but both curves display the same trends. The differences can be explained by the smaller resolution of the numerical model, leading to averaged but less accurate gradients. A more appropriate gradient calculation method would have been to first smooth the calculated and simulated temperature logs, then to derive from them more reliable temperature gradients. Such an improvement was beyond the scope of this work. Nevertheless, this first comparison allowed us to validate the numerical heat diffusion model and to confirm that the numerical simulations provide consistent results that can be compared with measured geothermal gradients in order to study the effects of flow paths onto the temperature distribution.

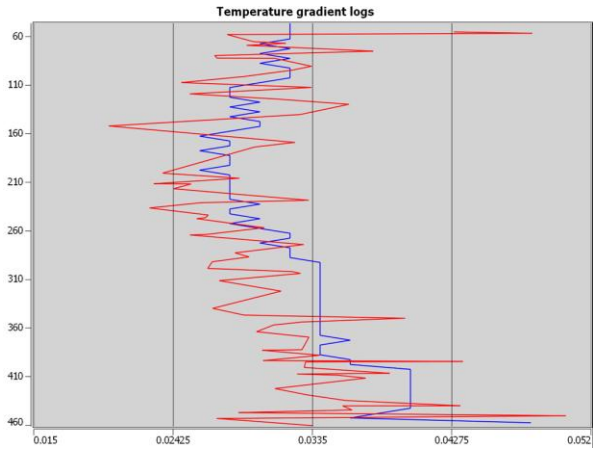

Figure 5: Comparison between the analytical temperature gradient (in °C/m) calculated using the Fourier law (in red), and the simulated temperature gradient for the hydrostatic conditions of scenario 1 (in blue).

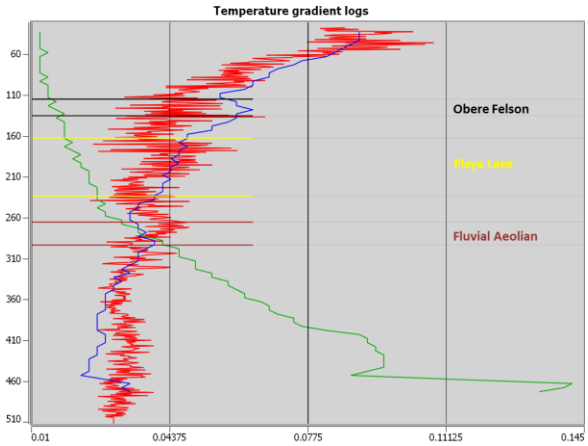

Figure 6: Comparison of the temperature gradient measured in well EPS1 (in red) with the simulated ones of scenario 2 (in green) and scenario 3 (in blue) at a distance of 40 m from the left-hand fault.

The numerical temperature gradients obtained with scenarios 2 and 3 are depicted in Figure 6 together with the measured temperature gradient. The numerical gradients correspond to a distance of 40 m from the left-hand fault, which is the location where best fit of the measured temperature gradient was obtained as detailed later. Comparison of the measured and simulated temperature gradients shows that scenario 2 leads to an opposite global gradient trend (gradient increasing with depth), unlike scenario 3, which correctly reproduces the global trend and most local trend changes. These preliminary results tend to show that a convective

heat transport only located in the faults cannot explain by itself the measured temperatures. The two faults must also be flow-connected through the permeable sedimentary layers to fit the trends.

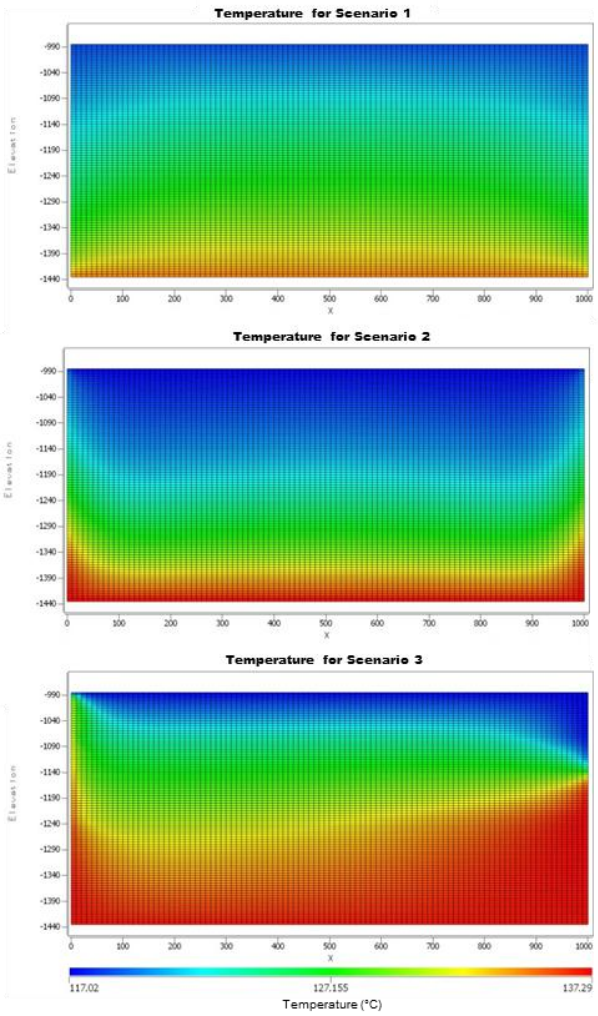

Figure 7: Simulated steady-state temperature distributions for scenario 1 (purely diffusive heat transfer), scenario 2 (convective heat transport in faults) and scenario 3 (convective heat transport in both faults and permeable layers).

The temperature distributions corresponding to scenarios 1 to 3 are illustrated in Figure 7. Whereas scenarios 1 and 2 lead to symmetrical temperature fields, scenario 3 reveals a more complex and non-symmetric temperature distribution, with higher vertical spreading of temperatures leftwards, i.e., downstream with respect to flows through the permeable sedimentary layers. With scenario 1, the faults have very little impact on the temperature distribution. This is not true with scenarios 2 and 3, for which the vertical distribution of temperature depends on the distance to the faults, with the possible exception of scenario 2, beyond a certain distance (say 100 m). More interesting, for scenario 3, it can be noticed that the vertical distribution of temperature can be used to determine whether the well is close to the downstream (left-hand) fault or the upstream (right-hand) one.

The only available measured temperature log is from borehole EPS1, which is known to be not too far from a fault and can therefore be used to understand the flow pattern and the flow direction at the fault block scale. To do so, the temperature data from EPS1 are compared with the simulated temperature logs at various distances from the faults (Figure 8). At all distances, the simulated temperature curves of scenario 2 are "concave" and do not fit the global trend of measured temperatures. On the contrary, the vertical temperature distributions predicted by scenario 3 depict the expected (convex) shape and correctly fit the measured temperature log, as well as the temperature gradient log (Figure 6), at a distance of 40 m from the left-hand (downstream) fault.

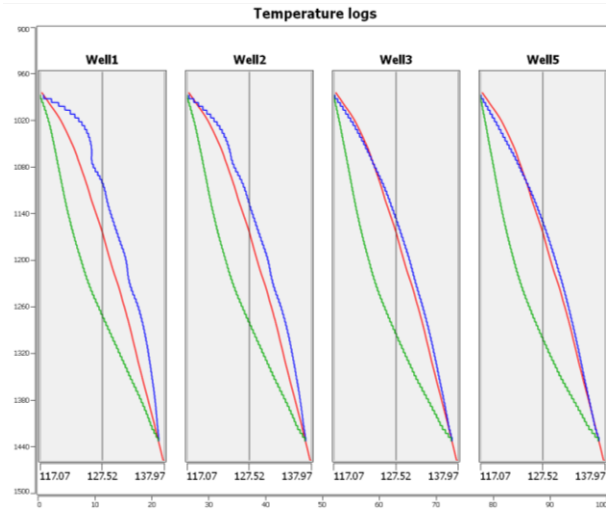

Figure 8: Three temperature logs at 10, 20, 40 and 80 m from the left-hand fault: measured temperature log (in red), simulated temperature log for scenario 2 (in green and simulated temperature log for scenario 3 (in blue).

Flow Pattern Results

Looking at the distribution of flow rates through the simulation grid cells in steady-state flow conditions for scenarios 2 and 3 (Figure 9), the flow paths can easily be interpreted.

As expected, scenario 2 only generates flows through the two faults, without any fluid exchange between the faults within the Buntsandstein formation, and scenario 3 gives rise to lateral flows through the three permeable sedimentary layers (Obere Felson as part of the Upper Buntsanstein, Playa Lake and fluvio-aeolian).

It can be noticed, however, that part of the fluids flowing through the sedimentary layers are likely to come from the overlying (necessarily warmer) aquifer(s) (Dezayes et al., 2007). Such an eventuality may be a concern to decide to produce geothermal fluids directly from the Buntsandstein formation.

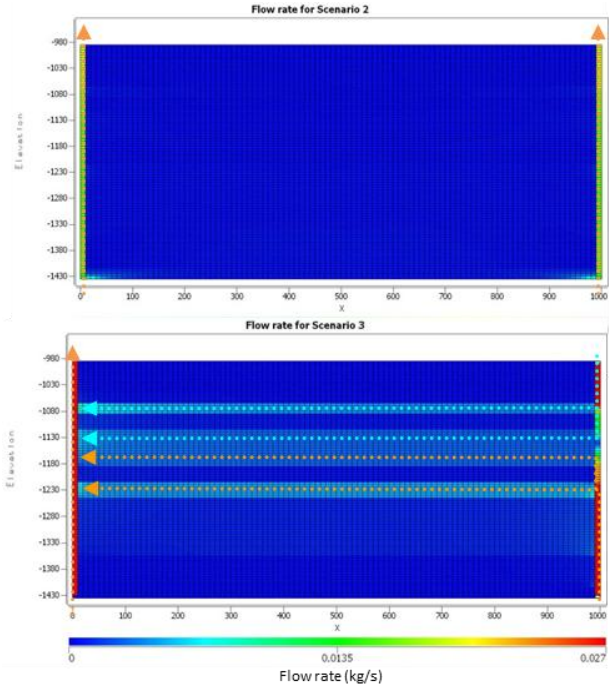

Figure 9: Steady-state fluid flow rate through the cells (kg/s) for scenario 2 (non-connected conductive faults) and scenario 3 (flow-connected conductive faults). The flow paths are indicated with arrows (orange for hot fluids coming from the bottom, light blue for warmer fluids coming from the top).

Influence of Prescribed Pressure Gradients

With no precise information being available about the pressure (or hydraulic potential) distribution in the granite reservoir and in the overlying aquifer, which are flow-connected by the faults, the simulation of scenario 3 was repeated with different pressure boundary conditions as indicated in Table 2.

For these new scenarios, the pressures prescribed at the top of the faults are the same as scenario 3. Only the bottom pressure conditions are changed. Though a more complete sensitivity analysis would have been required to explore more completely and methodologically the various flow condition situations, trend results can already be observed from these few additional simulations.

Compared with scenario 3, scenario 3.b involves smaller flow rates, whereas scenarios 3.c and 3.d correspond to higher and increasing flow rates. As seen from Figure 10, all the additional scenarios lead to temperature logs that further depart from the measured one. By decreasing the flow rates, too small temperatures are obtained, especially in the upper part of the model, whereas increased flow rates lead to excessive temperatures at all depths and all distances.

Table 2: Pressure and temperature boundary conditions applied to the top and the bottom of the model for the additional scenarios.

Scenario		*P (bar) left-hand fault*	*P (bar) right-hand fault*	*T (°C)*
3.b	Top BC	96	101=96+5	117
	Bottom BC	136	146=136+10	137
3.c	Top BC	96	101=96+5	117
	Bottom BC	155=136+19	165=136+29	137
3.d	Top BC	96	101=96+5	117
	Bottom BC	155=136+19	175=136+39	137

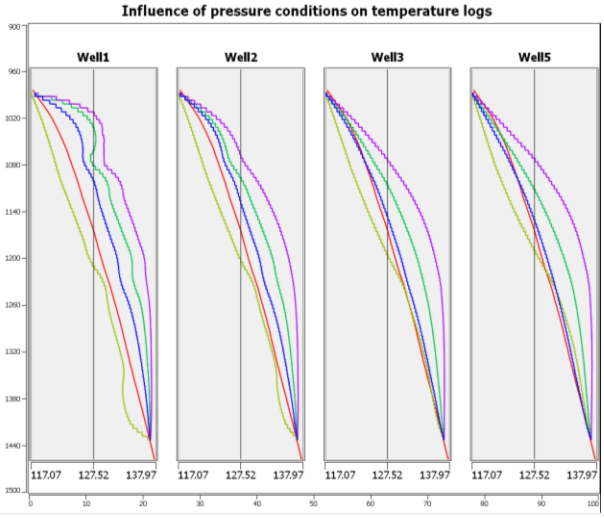

Figure 10: Influence of the flow boundary conditions on the temperature log at different distances of 10, 20, 40 and 80 m from the left-hand fault: measured temperature log (in red), scenario 3 (in purple), scenario 3.b (in yellow), scenario 3.c (in green) and scenario 3.d (in blue).

Among all simulated scenarios, scenario 3 best fits the measured temperatures and temperature gradient logs. Provided that the hydraulic properties assigned

to the faults and to the permeable sedimentary layers are appropriate, the hydraulic gradient of 0.005 bar/m applied between the faults (5 bars over a distance of 1,000 m) can be interpreted as resulting from a structural dip of about 3°.

Such a structural dip is consistent with those of about 5° measured in the Soultz-sous-Forêts area. It would result from the extensive tectonic history of the Upper Rhine Graben, which is formed by a set of blocks acting as horst and graben.

CONCLUSION

This phenomenological study was an attempt to understand and explain temperatures and temperature gradient anomalies observed in the Buntsandstein formation along borehole EPS1. It confirms the presence of convective heat transport through the crossing faults reaching the underlying granite reservoir, but also through several permeable stratigraphic layers connecting the faults. The flow boundary conditions of the numerical model (scenario) that best fits the temperature data can be explained by a structural dip of about 3°, which is consistent with the measured dips in the Soultz-sous-Forêts area.

From this study, information can also be derived about the distance of borehole EPS1 from the nearby fault and about the flow direction in the permeable layers with respect to this fault.

Further sensitivity analysis work is ongoing, however, to confirm that no other flow conditions, based on different hydraulic properties assigned to the faults or the litho-stratigraphic layers, on different pressure boundary conditions, or on both, can similarly reproduce the temperature data measured on borehole EPS1.

The numerical models also show that water coming from the overlying aquifer(s) can be drained by upstream faults and reach the permeable sedimentary layers where it mixes with flowing geothermal water coming from the granite reservoir. Whether such a phenomenon is critical to production of geothermal fluid directly from the Buntsandstein formation is an aspect that would need to be confirmed. It could be studied as part of a 3D numerical reservoir model in order to assess the geothermal potential of the reservoir, depending on the number, locations and rates of producer and injector wells.

AKNOWLEDGEMENTS

We thank TERANOV SAS, which financially supported part of this work.

REFERENCES

Bächler, D., Khohl, T., Rybach, L. (2003). "Impact of graben-parallel faults on hydrothermal convection - Rhine Graben case study," *Physics and Chemistry of the Earth*,: **28** (9-11): 431-441.

Caine, J.S., Evans, J.P., Forster, C.B. (1996). "Fault zone architecture and permeability structure," *Geology*, **24**: 1025-1028.

Dezayes, C., Thinon, I., Courrioux, G., Tourlière, B., Genter, A. (2007). "Estimation du potentiel géothermique des réservoirs clastiques du Trias dans le Fossé rhénan," *Rapport Final*. BRGM/**RP-55729-FR**: 72p.

Genter, A., Guillou-Frottier, L., Breton, J.P., Denis, L., Dezayes, C., Egal, E., Feybesse, J.L., Goyeneche, O., Nicol, N., Quesnel, F., Quinquis, J.P., Roig, J.Y., Schwartz, S. (2004). "Typologie des systèmes géothermiques HDR/HFR en Europe," *Rapport final*. BRGM/**RP-53452-FR**, 165 p., 75 fig., 10 tab.

Genter, A., Traineau, H., Ledésert, B., Bourgine, B. and Gentier, S. (2000). "Over 10 years of geological investigations within the HDR Soultz project, France," *World Geothermal Congress*.

Haffen, S., Geraud, Y., Diraison, M. and Dezayes, C. (2013), "Fluid-flow zones in a geothermal sandstone reservoir: localization from thermal conductivity and temperature logs, borehole EPS1 (Soultz-sous-Forêts, France)," *Geothermics*, **46**: 32-41

Haffen, S. (2012), "Caractéristiques géothermiques du réservoir gréseux du Buntsandstein d'Alsace," *Thèse de doctorat de l'Université de Strasbourg* : 393p.

Kohl, T., Bächler, D. and Rybach, L. (2000), "Steps towards a comprehensive thermo-hydraulic analysis of the HDR test site Soultz-sous-Forêts," *World Geothermal Congress*.

Le Carlier, C, JJ. Royer, and Flores, E.L. (1994), "Convective heat transfer at the Soultz-sous-Forêts Geothermal Site: Implications for oil potential," *First Break*, **12**:553-560.

Ledésert, B., and Hébert, R. (2012), "The Soultz-sous-Forêts' Enhanced Geothermal System: A Granitic Basement Used as a Heat Exchanger to Produce Electricity," *Heat Exchangers*.

Place, J., Diraison, M., Naville, C., Geraud, Y., Schaming, M., Dezayes, C. (2010), "Decoupling of deformation in the Upper Rhine Graben sediments. Seismic reflection and diffraction on 3-component Vertical Seismic Profiling (Soultz-sous-Forets area)," *Comptes Rendus Geoscience*, **342**: 575-586.

Pribnow, D., Schellschmidt, R. (2000), "Thermal tracking of upper crustal fluid flow in the Rhine Graben," *Geophysical Research Letters*, **27**: 1957-1960.

Pruess, K., Oldenburg, C. and Moridis, G. (1999), "TOUGH2 User's Guide, Version 2.0," *Lawrence Berkeley National Laboratory Report, LBNL-43134*.

Sizun, J.P., Jeannette, D. (1995), "Transformations pétrographiques succéssives conduisant à la structuration des réservoirs du Buntsandstein : le forage géothemique EPS1 de Soultz-sous-Forêts (Alsace, France)," *Compte Rendu de l'Academie des Sciences - serie IIA*, **320**: 365-372.

Vernoux, J.F., Genter, A., Razin, P., Vinchon, C. (1995), "Geological and petrophysical parameters of a deep fractured sandstone formation as applied to geothermal exploitation, EPS-1 borehole, Soults-sous-Forêts, France". *BRGM Open file Report*, **R 38622**: 69 p.